Nitrile-Imine Crosslinking in Peptide Ions with Aromatic Amino Acid Residues: Are Ring-Stacking Interactions Important?

Chenxun Dai

A Thesis

submitted in partial fulfillment of the

requirements for the degree of

Master of Science

University of Washington

2026

Committee:

František Tureček

Bo Zhang

Program Authorized to Offer Degree:

Department of Chemistry

University of Washington

Abstract

Nitrile-Imine Crosslinking in Peptide Ions with Aromatic Amino Acid Residues: Are Ring-Stacking Interactions Important?

Chenxun Dai

Chair of the Supervisory Committee:

František Tureček

Department of Chemistry

In this study, a series of diaryltetrazole–peptide conjugates containing aromatic amino acid residues were studied by ultraviolet photodissociation (UVPD) mass spectrometry. Upon irradiation at 213 nm and in the 250–290 nm range, the tetrazole unit underwent selective loss of molecular nitrogen (N_2) to generate reactive nitrile-imine intermediates. These intermediates subsequently participated in intramolecular cross-linking reactions, primarily involving peptide backbone amide groups, leading to macrocyclic product ions.

Product structures and dissociation pathways were proposed based on tandem mass spectrometry experiments, including UVPD-MS^2 and collision-induced dissociation (CID-MS^3). High-resolution ion mobility measurements were performed to determine experimental collision cross sections, providing structural information for both precursor and denitrogenated ions.

Theoretical calculations were performed to support structural assignments and mechanistic interpretation. Conformational searches were conducted using Born–Oppenheimer molecular dynamics (BOMD), and density functional theory (DFT) computations were used to optimize geometries and evaluate relative energies of low-energy isomers. Time-dependent DFT calculations were further used to analyze electronic transitions and rationalize wavelength-dependent photodissociation behavior.

Based on combined experimental and computational results, the mechanistic understanding of nitrile-imine cross-linking was refined. The results indicate that ground-state aromatic stacking interactions are not universally required for cross-link formation, while differences in excited-state electronic structures are more likely responsible for the observed wavelength-dependent photochemical behavior.

ACKNOWLEDGEMENTS

First, I would like to sincerely thank my advisor, Professor František Tureček. Throughout my master's studies, Professor Tureček has always provided me with generous guidance, trust, and support. One year ago, when I felt confused about my future, his passion for scientific research inspired me and encouraged me to continue exploring and moving forward in chemistry. His extensive knowledge, sharp scientific insight, and rigorous attitude toward science not only contributed greatly to the completion of my thesis but also helped me understand how to become a researcher.

Through my research training in his group, I learned not only mass spectrometric analysis, fragmentation mechanisms, and related theoretical methods, but also how to identify questions from experimental observations, develop hypotheses, and evaluate them using evidence. These experiences will remain among the most valuable parts of my future scientific journey.

I would also like to thank Dr. Martin Sadílek, manager of Mass Spectrometry Facility of the Department of Chemistry, for his technical support and assistance. His experience and professional advice in the instruments provided important support for the successful completion of my relevant work.

I would especially like to appreciate Sizhong Shen and Chenyang Wei for their help when I first joined the group. They patiently introduced me to the laboratory environment, instrument operation, and the group's research directions, allowing me to successfully

transition from organic synthesis to mass spectrometric analysis. Their support provided a strong foundation for my subsequent research.

I would also like to express my special thanks to Ph.D. student Yingxuan “Mars” Wei and postdoctoral researcher Dr. Simona Sedláčková. Throughout this project, they generously provided me with help and support. They devoted considerable time and effort to guiding me in experimental design, data analysis, instrument operation, and discussions of research ideas. Many of the experimental skills, research experience, and problem-solving approaches I have developed would not have been possible without their help and patient guidance.

In addition, I sincerely thank all the researchers and collaborators who contributed to this study. Communicating and working with researchers from different academic backgrounds not only supported the progress of this work but also greatly broadened my academic perspective and deepened my understanding of the importance of interdisciplinary collaboration in modern scientific research.

Finally, I would like to express my deepest gratitude to my parents for their understanding, trust, and support throughout the years. They have always been my strongest source of support, both in my daily life and emotionally. I would also like to thank all the friends who have accompanied and helped me in Seattle and back home. It is because of your encouragement and support that I have been able to complete this meaningful and unforgettable academic journey. I dedicate this thesis to everyone who has supported and helped me along the way.

TABLE OF CONTENTS

LIST OF FIGURES

LIST OF TABLES

Chapter 1. Introduction

1.1 Overview of Photochemical Crosslinking

Protein–protein and protein–nucleic acid interactions play important roles in many biological processes, including DNA replication, transcriptional regulation, and RNA processing.[1] To characterize these interaction interfaces at the molecular level, crosslinking techniques have been widely used to convert transient noncovalent interactions into stable covalent linkages, enabling the investigation of the structures and interaction sites of biomolecular complexes.[2]

Traditional crosslinking methods generally rely on chemical crosslinkers that react with specific functional groups, mainly including primary amines, carboxyl groups, and thiol groups on amino acid side chains.[3] By forming covalent links within or between molecules, crosslinking reactions can not only stabilize dynamic and transient biomolecular interactions but also provide important information for subsequent structural analysis. To date, the applications of crosslinking have expanded from traditional molecular modification to various areas of the life sciences, including biomaterial construction, drug delivery, and structural studies of biomolecules.[4] Among these applications, crosslinked hydrogels have shown considerable potential in drug delivery and tissue engineering because of their good biocompatibility and tunable physicochemical properties.[5] In addition, crosslinking strategies are playing an increasingly important role in the structural characterization of proteins and other biomolecules.[6]

In contrast, photochemical crosslinking adopts ultraviolet irradiation to generate highly reactive intermediates, such as radicals, carbenes, nitrenes, and nitrile imines. These intermediates can react with neighboring molecules within an extremely short time, allowing interaction sites that are spatially close to be preferentially captured.[7,8] Because these methods generally do not require the introduction of long spacer arms, they provide high spatial selectivity while causing relatively less disturbance to the original conformations of biological systems. In addition, the stable covalent products generated through photochemical crosslinking provide an important basis for subsequent mass spectrometric analysis, allowing crosslinking sites and interaction regions to be identified.[7,9]

Commonly used photochemical crosslinking groups nowadays include diazirine- and benzophenone-based systems. Upon ultraviolet irradiation, these systems generally generate carbene or diradical intermediates, which subsequently react with nearby molecules.[10,11] However, because intermediates such as carbenes are highly reactive, they can readily undergo nonselective side reactions. Some systems also have limitations such as low reaction efficiency and long irradiation times.

Nitrile imines have long been known as reactive 1,3-dipoles capable of undergoing cycloaddition reactions with various dipolarophiles.[12] In 2008, Song et al. applied this established reactivity to biological systems by developing a photoinduced 1,3-dipolar cycloaddition based on 2,5-diaryltetrazoles. Upon ultraviolet irradiation, the tetrazoles generated nitrile-imine intermediates that reacted with alkene dipolarophiles, enabling the rapid and selective derivatization of tetrazole-containing proteins.[13] This work demonstrated

the utility of tetrazole photochemistry for biomolecular modification rather than representing the initial discovery of nitrile-imine addition chemistry.

In recent years, nitrile-imine photochemistry has gradually developed into a versatile and controllable tool for biomolecular derivatization.[8,14] In addition to traditional alkene dipolarophiles, studies have shown that amide groups, carboxyl groups, and certain nitrogen-containing functional groups can also participate in these reactions. For example, Zhao et al. reported that diaryltetrazoles could undergo photoinduced coupling reactions with carboxylic acids in aqueous solution and further applied this reaction to protein labeling, demonstrating that these systems are not limited to traditional alkene dipolarophiles.[15] In addition, under specific conditions, diaryltetrazoles can react with primary amines to form triazole products, further expanding the types of reactions and the range of applications of this system.

Nitrile-imine-mediated crosslinking has also been demonstrated in biomolecular systems. Herner et al. developed 2-aryl-5-carboxytetrazoles as photoaffinity labels for drug-target identification,[16] and Tian et al. subsequently reported genetically encoded 2-aryl-5-carboxytetrazoles for site-selective protein photo-crosslinking.[17]

1.2 Development and Challenges of Crosslinking Mass Spectrometry (XL-MS)

With the rapid development of high-resolution mass spectrometry, tandem mass spectrometry, and related data analysis methods, crosslinking mass spectrometry (XL-MS) has become an important technique for studying higher-order protein structures and protein interactions.[2,18] XL-MS introduces covalent crosslinks between amino acid residues that are

spatially close and identifies the resulting crosslinked peptides by tandem mass spectrometry, thereby providing distance constraints within proteins and protein complexes.[19] By inducing peptide fragmentation through MS/MS and analyzing the resulting fragment ions, peptide sequences, amino acid modifications, and side-chain changes can be further identified.[18] This structural information can be combined with techniques such as cryogenic electron microscopy (cryo-EM), nuclear magnetic resonance (NMR), and computational modeling, providing important evidence for protein conformational analysis, studies of protein–protein interactions, and characterization of dynamic structural changes.

Despite significant recent advances in XL-MS instrumentation, crosslinker design, and bioinformatic analysis, many challenges remain in their development.[20] Different crosslinking systems still vary considerably in their reaction mechanisms, crosslinking-site selectivity, and data analysis workflows. These differences not only make it more difficult to compare and validate experimental results but also limit the development and wider application of new crosslinking strategies.[21] Therefore, developing new photochemical crosslinking systems with higher reaction selectivity, easier structural characterization, and compatibility with complex biological systems remains an important research direction in the field of XL-MS.

In recent years, the Tureček group has systematically investigated the reactivity of nitrile imines under gas-phase conditions,[8] with particular emphasis on their diverse reaction pathways in the mass spectrometric environment, including intramolecular crosslinking reactions with functional groups such as amides, carboxyl groups, and nucleobases. Wan et al. first demonstrated that nitrile-imine intermediates generated by the photolysis of

diaryltetrazoles could form stable macrocyclic crosslinked structures in gas-phase peptides and peptide–nucleic acid complexes. These structures could be characterized using UVPD, CID, and ion mobility mass spectrometry.[22] Subsequently, Vlk et al. further expanded the reaction scope of this system and found that amino acid side-chain functional groups in Asp, Glu, Asn, and Gln could also participate in nitrile-imine crosslinking reactions, further demonstrating the reaction diversity of this gas-phase photocrosslinking system.[23] Based on these previous studies, the present work further investigates the effects of aromatic residues on diaryltetrazole photochemistry and nitrile-imine crosslinking efficiency.[24]

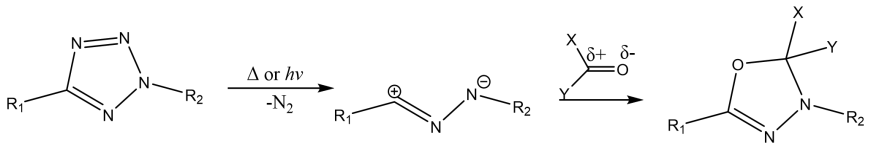

Figure 1. Reaction scheme of tetrazole photolysis and nitrile-imine cycloaddition.

1.3 Research Motivation and Scope

Although previous studies have demonstrated that nitrile imines can undergo gas-phase crosslinking reactions with various functional groups, the role of aromatic amino acid residues in these systems has not yet been systematically investigated. Aromatic side chains may not only influence the gas-phase conformations of peptide ions through π–π interactions but also participate in electronic transitions and energy-transfer processes upon UV excitation, thereby affecting wavelength-dependent photodissociation behavior and subsequent crosslinking pathways.

In solution, stacking interactions between aromatic rings (π–π stacking) have been extensively studied and are considered closely related to protein structural stability and

molecular recognition processes.[25] However, under gas-phase conditions, the absence of solvent effects may result in substantial differences in the conformations and aromatic interactions of charged peptide ions compared with those in solution.[26,27] It remains unclear whether aromatic side chains and diaryltetrazole groups form stable stacked structures and whether such interactions affect the efficiency and selectivity of nitrile-imine crosslinking reactions.

On the other hand, UV excitation at different wavelengths may correspond to different types of electronic transitions.[28] For tetrazole–peptide systems containing aromatic amino acid residues, aromatic side chains may participate in excited-state processes in addition to the π–π* transitions of the tetrazole group itself, thereby affecting energy distribution and subsequent fragmentation behavior. Therefore, investigating the effects of different aromatic residues and excitation wavelengths on UVPD behavior can provide further insight into the mechanism of gas-phase nitrile-imine crosslinking.

In this study, a series of tetrazole–peptide conjugates containing aromatic amino acid residues, including Phe, Tyr, Trp, and their substituted derivatives, were used as model systems. Their photodissociation behavior, crosslinked product structures, and possible excited-state processes were systematically investigated using UVPD-MS, CID-MS^3, high-resolution ion mobility mass spectrometry, and theoretical calculations. By combining experimental results with theoretical calculations, this study aims to elucidate the roles of aromatic interactions and excited-state electronic structures in gas-phase nitrile-imine

crosslinking and to further refine the mechanistic understanding of these photochemical crosslinking systems.

Chapter 2. Experimental Section

2.1 Peptide Synthesis

A series of model pentapeptides with the general sequence XAAAK (X = Tyr, Phe, or Trp), arranged from the N-terminus to the C-terminus, were designed and synthesized. The peptide chains were assembled on Wang resin using Fmoc-based solid-phase peptide synthesis and standard coupling procedures.[29]

During synthesis, the lysine residue was initially anchored to the Wang resin, after which a 2,5-diaryltetrazole carbonyl group was introduced at its side-chain ε-amino group. Following side-chain modification, peptide elongation was continued through the sequential coupling of alanine (Ala) residues and the N-terminal amino acid (X = Tyr, Phe, or Trp), yielding the target tetrazole-labeled peptides. The resulting peptides are denoted as XAAA-tet-K; for example, YAAA-tet-K represents a peptide with an N-terminal tyrosine residue and a tetrazole group attached to the side chain of the C-terminal lysine residue (Figure 2).

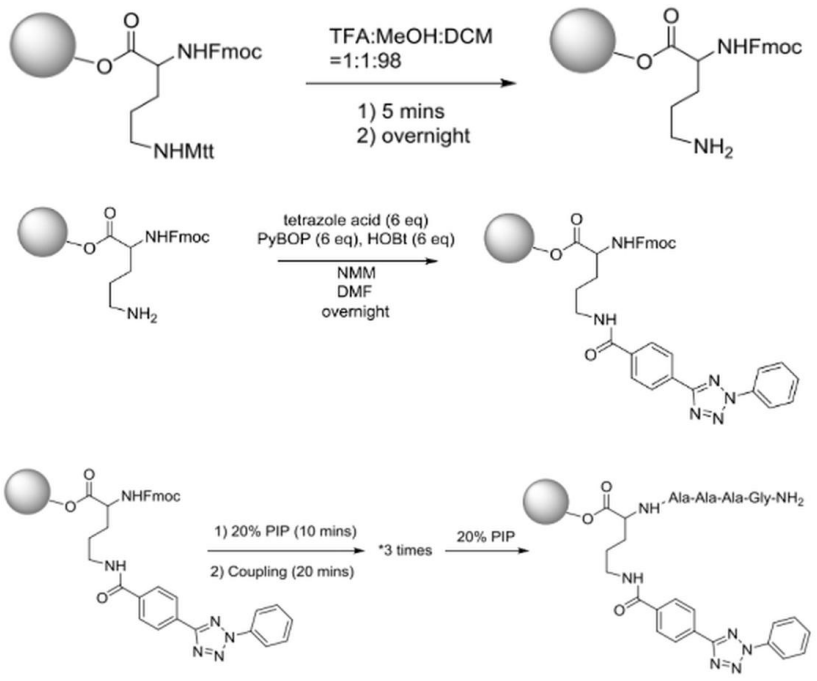

Figure 2. Solid-phase synthesis of tetrazole-modified peptides

The 2,5-diaryltetrazoles and their substituted derivatives used in this study, including the 4-NO_2- and 4-MeO-substituted systems, were synthesized according to a previously reported method, with appropriate modifications for the different substituents.[11]

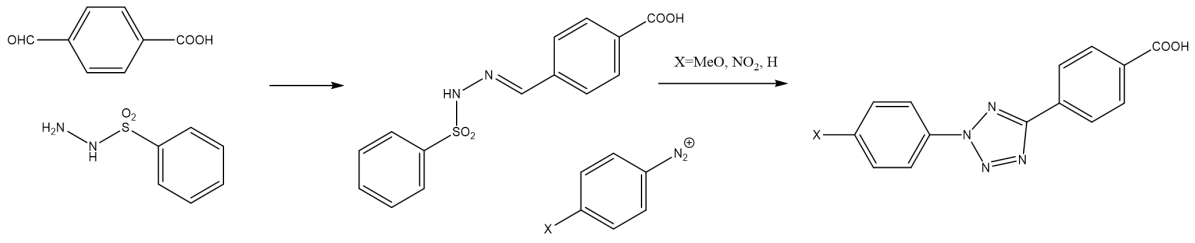

Figure 3. Synthesis of substituted diaryltetrazole benzoic acids.

2.2 Mass Spectrometry Experiments

Mass spectrometry experiments were performed on a Thermo Fisher Orbitrap Ascend high-resolution mass spectrometer. Samples were dissolved in an acetonitrile/water mixture

(ACN/H_2O, 1:1, v/v) and introduced into the gas phase by electrospray ionization (ESI) in positive-ion mode, generating protonated molecular ions, $[M+H]^+$.

The photolysis of diaryltetrazoles and the formation and structural characterization of subsequent crosslinked products were primarily investigated using ultraviolet photodissociation (UVPD) and collision-induced dissociation (CID) mass spectrometry. In the UVPD experiments, selected precursor ions were irradiated with a 213 nm UV laser, while wavelength-dependent experiments were conducted using tunable UV light in the 250–290 nm range. Upon UV irradiation, the diaryltetrazole group underwent N_2 loss to generate a highly reactive nitrile-imine intermediate, which subsequently formed intramolecular crosslinked products (Figure 1). The resulting product and fragment ions were detected and analyzed using the high-resolution Orbitrap mass analyzer.

To further investigate the conformational characteristics of gas-phase peptide ions and possible interactions between aromatic rings, cyclic traveling-wave ion mobility mass spectrometry (cIMS-MS) was used to analyze the structures of the precursor ions and their denitrogenated products. Experimental collision cross sections (CCSexp) were obtained by measuring the arrival times of the ions in the mobility region and calibrating them using poly-DL-alanine standards. The calculated collision cross sections (CCScalc) of the theoretical structures were then compared with the corresponding CCSexp values to evaluate the plausibility of different candidate conformations and to assess whether stable π–π stacking interactions existed between the aromatic side chains and diaryltetrazole groups.

2.3 Computational Methods

To further elucidate the gas-phase conformations and photochemical behavior of tetrazole–peptide ions, molecular dynamics simulations, density functional theory calculations, and excited-state electronic structure analyses were combined to systematically investigate these systems.

Born–Oppenheimer molecular dynamics (BOMD) was first used to perform conformational searches of the protonated peptide ions and identify possible gas-phase structures. Representative structures selected from these searches were subsequently subjected to density functional theory (DFT) calculations, including geometry optimization and energy analysis, to obtain stable low-energy conformers. To determine whether the calculated structures accurately represented the experimentally observed ion conformations, theoretical collision cross sections (CCS_{calc}) were calculated for the candidate structures and compared with the experimental collision cross sections (CCS_{exp}) obtained from ion mobility measurements. The spatial conformations of the peptide ions and the structures of the crosslinked products were then analyzed by combining the experimental and theoretical results.

To investigate the effects of aromatic residues on tetrazole photochemistry, time-dependent density functional theory (TD-DFT) was further employed to analyze the excited-state properties of these systems. Electronic transitions, excitation energies, and molecular orbital distributions were calculated to examine how the aromatic side chains and tetrazole substituents affect UV absorption and photodissociation processes and to explain the

experimentally observed differences in wavelength-dependent photodissociation efficiencies and fragmentation behavior.

All theoretical calculations were performed according to an established computational workflow, including initial conformational screening assisted by semiempirical methods, DFT geometry optimizations and energy calculations, theoretical CCS calculations, and TD-DFT excited-state analyses. Together, these methods enabled a comprehensive investigation of the structures and photochemical properties of the gas-phase ions.

Chapter 3. Results and Discussion

3.1 UVPD Behavior of XAAA-tet-K Conjugates

To investigate the effects of aromatic amino acid residues on diaryltetrazole photochemistry, a series of XAAA-tet-K peptide conjugates were first analyzed by ultraviolet photodissociation (UVPD). Here, X represents Phe, Tyr, or Trp, corresponding to the precursor ions FAAA-tet-K (m/z 755), YAAA-tet-K (m/z 771), and WAAA-tet-K (m/z 794), respectively (Figure 4).

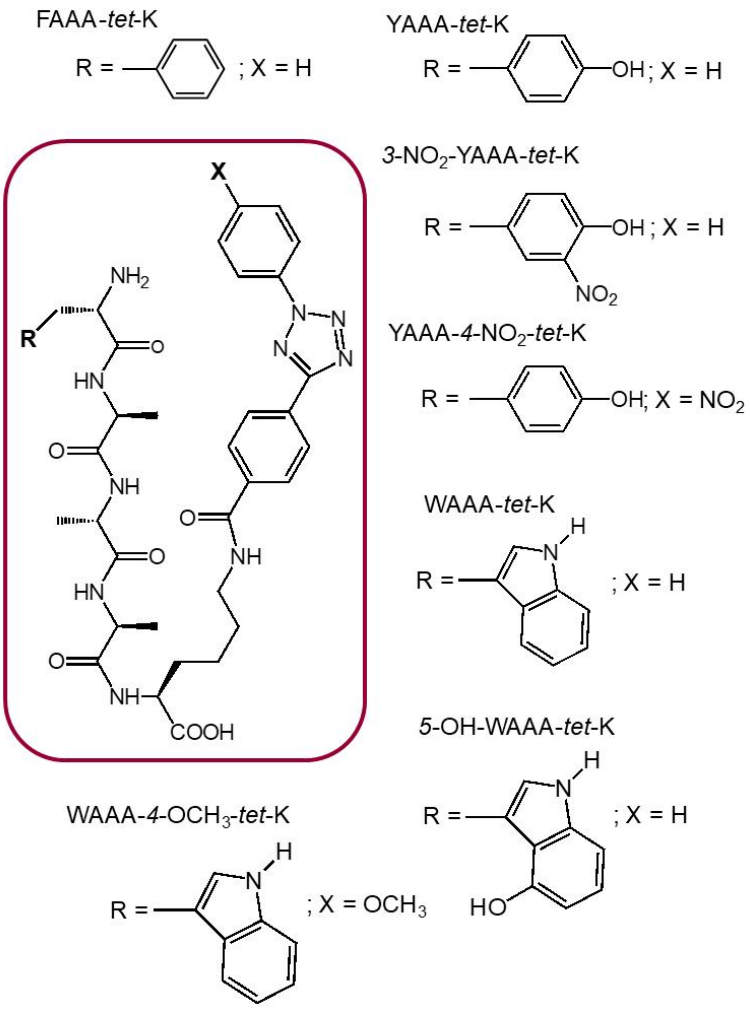

Figure 4. Structures of the diaryltetrazole–peptide conjugates

Under electrospray ionization conditions, these peptide conjugates were predominantly observed as singly charged $[M+H]^+$ ions. Following mass selection, the precursor ions were irradiated at 213 nm and within the 250–290 nm range to investigate the photodissociation behavior of the tetrazole group under different excitation conditions.

In all systems, UVPD effectively induced N_2 loss from the diaryltetrazole group, generating the corresponding $[M+H-N_2]^+$ ions, although the photodissociation yields at 213 nm varied among the conjugates. This process involves the loss of an N_2 molecule from the tetrazole ring to form a highly reactive nitrile-imine intermediate and represents the key

initial step in the subsequent crosslinking reaction. Prominent product peaks associated with N_2 loss were observed for FAAA-tet-K, YAAA-tet-K, and WAAA-tet-K, demonstrating that tetrazole photolysis occurs under gas-phase conditions.

In addition to N_2 loss, UVPD induced further fragmentation processes (Figure 5). Upon excitation at 213 nm, multiple b- and y-type fragment ions arising from peptide backbone cleavage were observed together with the $[M+H-N_2]^+$ ions. Notably, characteristic ions such as $[y_1+2H]^+$, $[y_2+2H]^+$, and $[y_3+2H]^+$ appeared in the spectra instead of the more commonly observed $[y_n+H]^+$ ions (Figure 6). These results indicate that, in addition to promoting tetrazole photolysis, high-energy UV excitation may induce peptide bond cleavage through energy redistribution, resulting in competing backbone fragmentation.

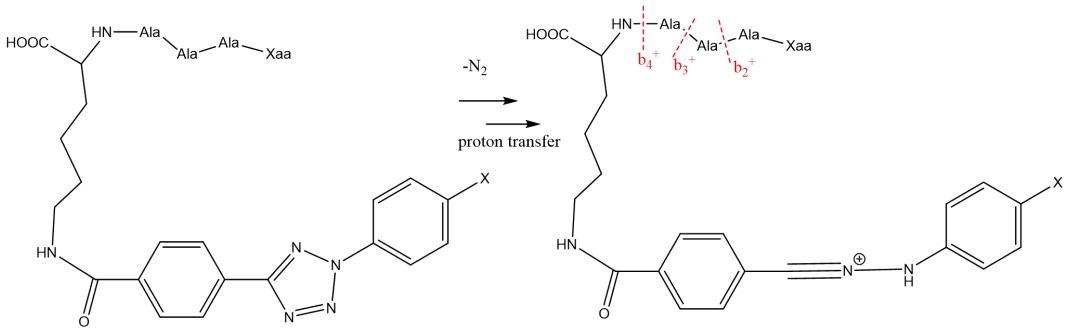

Figure 5. Nitrile-imine formation and backbone fragmentation.

The systems exhibited markedly different fragmentation characteristics at different excitation wavelengths. For WAAA-tet-K, ions associated with N_2 loss and backbone cleavage were both observed under 213 nm UVPD conditions, whereas backbone fragmentation was substantially reduced upon UVPD near 280 nm, with fragmentation occurring predominantly through the tetrazole N_2-loss channel (Figure 6). Similar trends were observed for FAAA-tet-K and YAAA-tet-K. These results indicate that excitation at longer

wavelengths more selectively targets the tetrazole chromophore and thereby promotes N_2 loss, whereas excitation at 213 nm more readily induces competing high-energy fragmentation processes.

Further comparison of the systems containing different aromatic residues showed that, although tetrazole photolysis occurred in all three systems, their fragmentation behavior was not identical. YAAA-tet-K exhibited relatively high selectivity for tetrazole photolysis, whereas WAAA-tet-K displayed a more complex fragmentation pattern, with more backbone- and side-chain-related fragment ions observed in addition to products associated with N_2 loss. The overall behavior of FAAA-tet-K was intermediate between those of the other two systems.

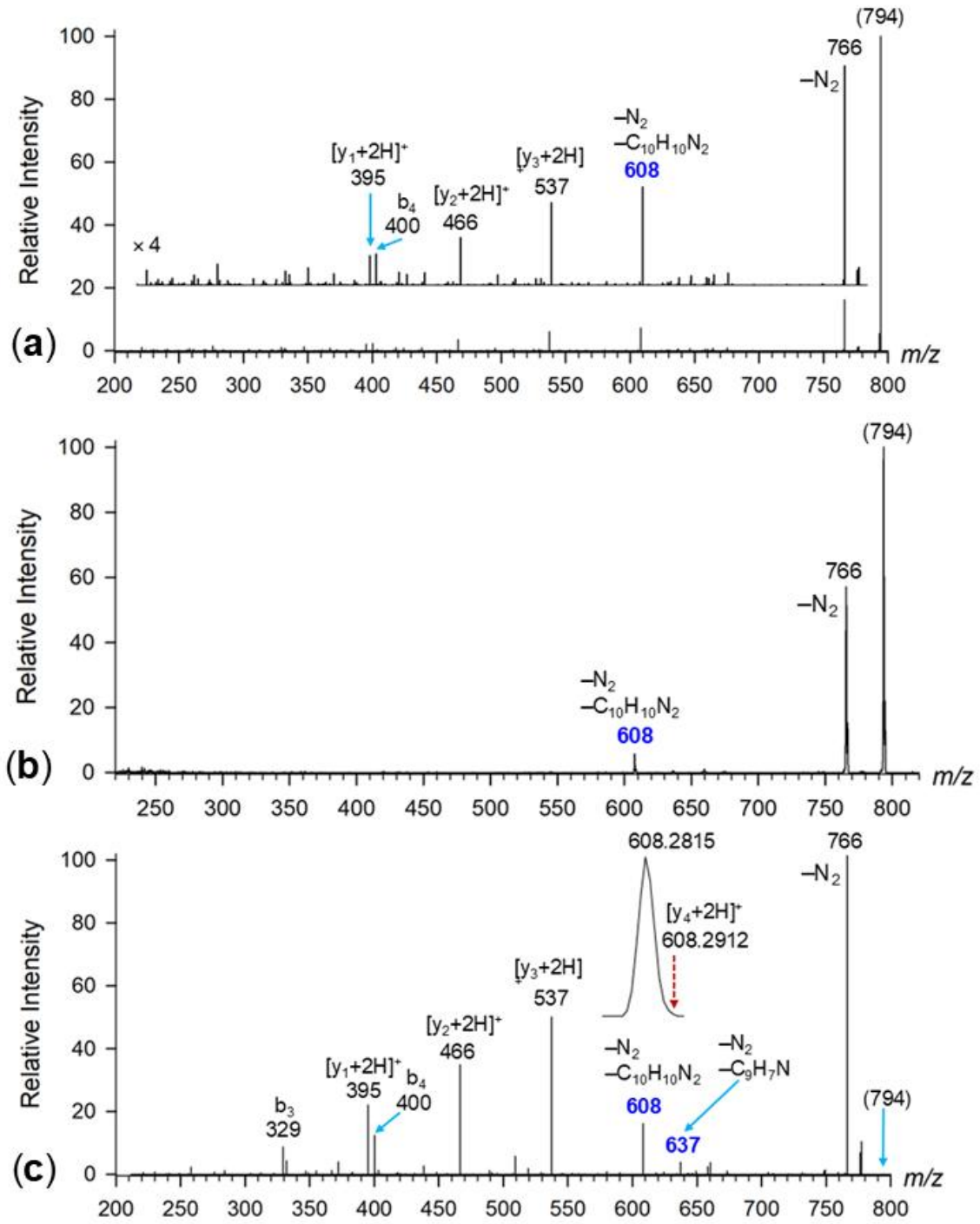

Figure 6. (a) 213 nm UVPD-MS², (b) 280 nm UVPD-MS², and (c) CID-MS² spectra of $(WAAA\text{-}tet\text{-}K + H)^+$ ions (m/z 794). The inset shows the accurate-mass profile of the m/z 608 ion.

These results demonstrate that different aromatic residues influence the energy distribution and fragmentation pathways of tetrazole–peptide conjugates upon UV excitation.

However, the specific structures of the denitrogenated products cannot be determined from the UVPD results alone, nor can these results establish whether the aromatic side chains affect subsequent crosslinking through intramolecular aromatic interactions. Therefore, CID-MS^3 experiments, ion mobility mass spectrometry, and theoretical calculations were further combined to investigate the structures and reaction mechanisms of the denitrogenated products. Although efficient tetrazole photolysis occurred in all systems containing aromatic residues, the observed differences in wavelength-dependent fragmentation suggest that these residues may not merely serve as structural components but may also participate in excited-state energy distribution and modulate subsequent fragmentation processes.

3.2 Structural Evidence for Nitrile-Imine Crosslinked Ions

To further investigate the structural characteristics of the ions generated by UVPD, the denitrogenated $[M+H-N_2]^+$ ions were analyzed by CID-MS^3, and the major fragmentation products were structurally characterized using high-resolution accurate mass measurements (Figures 7-9).

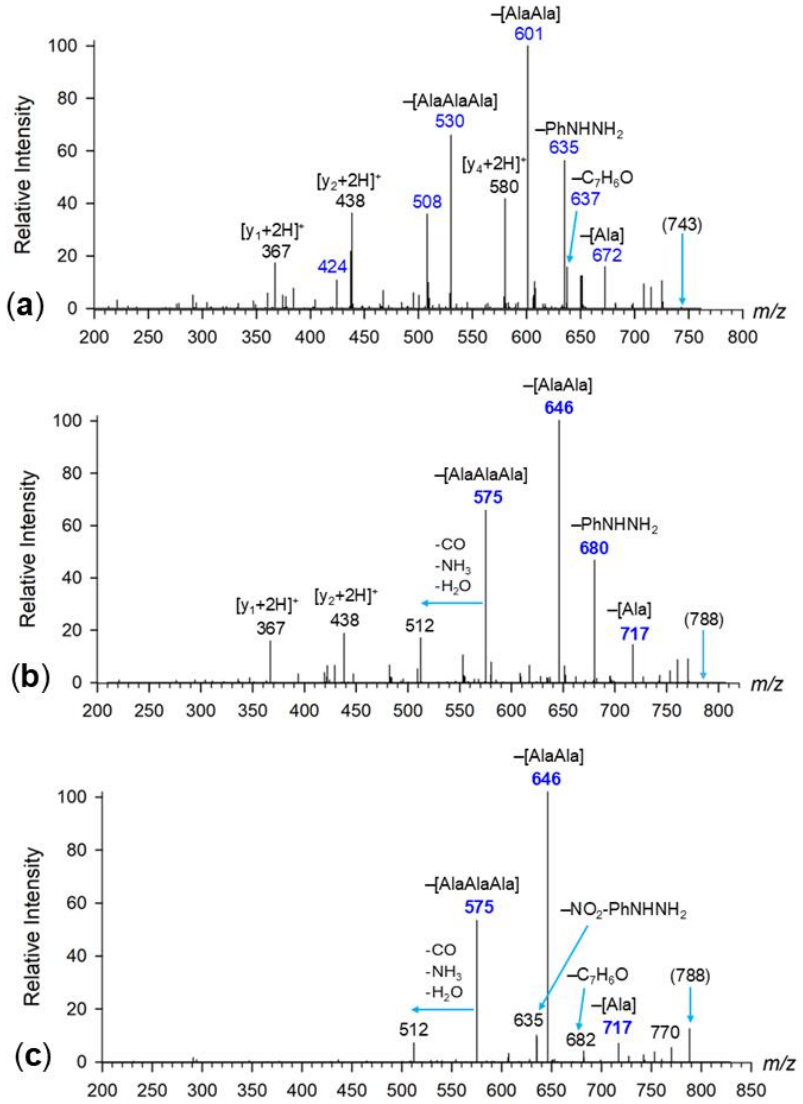

Figure 7. UVPD-CID-MS³ spectra of denitrogenated YAAA-tet-K conjugates: (a) YAAA-tet-K, (b) 3-NO_2-YAAA-tet-K, and (c) YAAA-4-NO_2-tet-K.

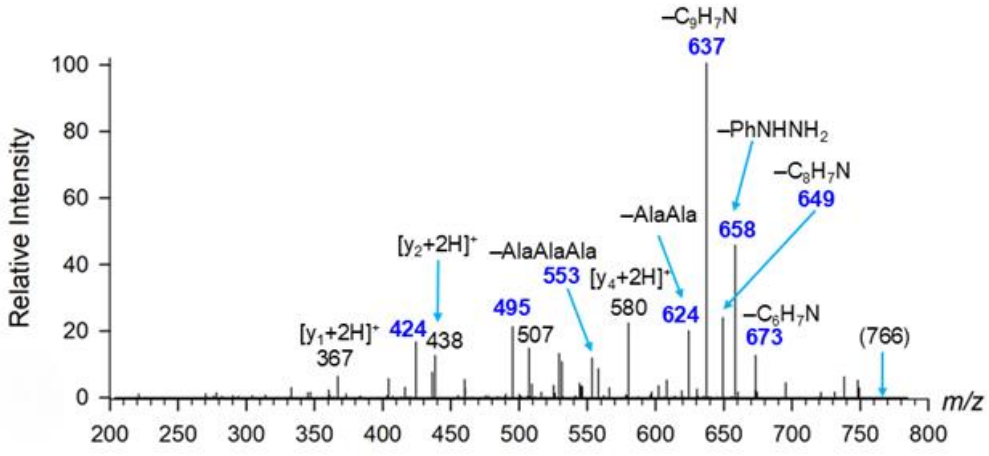

Figure 8. UVPD-CID-MS³ spectrum of denitrogenated WAAA-tet-K.

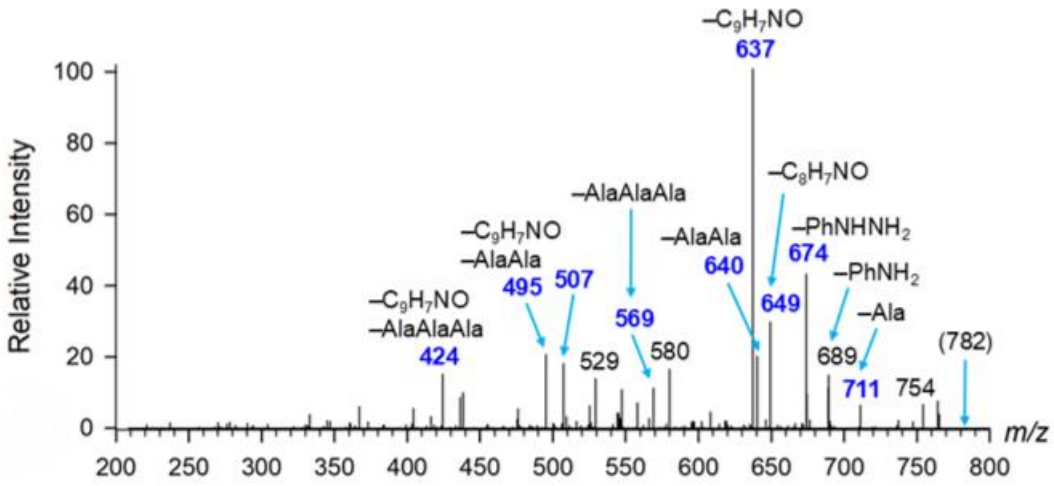

Figure 9. UVPD-CID-MS³ spectrum of denitrogenated 5-OH-WAAA-tet-K

The CID-MS³ results showed that the different aromatic systems exhibited highly similar fragmentation behavior following N_2 loss. A series of common characteristic fragment ions were observed for FAAA-tet-K, YAAA-tet-K, and WAAA-tet-K, indicating that these denitrogenated products share similar structural features and may arise from a common nitrile-imine reaction pathway.

One important common feature was the neutral loss of phenylhydrazine. Characteristic ions such as m/z 635 were observed for YAAA-tet-K, and similar fragmentation behavior occurred in the FAAA-tet-K and WAAA-tet-K systems, including the m/z 658 ion of WAAA-tet-K (Figure 8). The consistent occurrence of this fragmentation process across multiple systems indicates that the denitrogenated products formed after UVPD retain similar tetrazole-derived structural motifs and undergo further dissociation through related pathways.

In addition to phenylhydrazine loss, the CID-MS³ spectra showed several sequential neutral losses associated with Ala residues. For example, both YAAA-tet-K and WAAA-tet-K produced fragment ions corresponding to Ala loss (Figures 7-9). Unlike the

b/y-type backbone fragment ions typically generated by CID of linear peptides, these sequential amino acid residue losses are more characteristic of internal residue losses from macrocyclic structures. This finding indicates that the nitrile-imine intermediates formed following UVPD-induced N_2 loss can undergo further intramolecular crosslinking reactions to generate stable macrocyclic crosslinked ions.

In addition, high-resolution mass spectrometry (HRMS) measurements further supported this interpretation. The experimentally measured masses were in good agreement with the theoretical values, allowing the elemental compositions of the major fragment ions to be reliably confirmed. Together with the observed CID fragmentation patterns, these results suggest that the nitrile-imine intermediates generated by tetrazole photolysis undergo intramolecular reactions with amide groups in the peptide backbone under gas-phase conditions, forming relatively stable macrocyclic crosslinked structures. During subsequent CID, these macrocyclic structures dissociate through characteristic pathways to produce a series of commonly observed diagnostic ions.

To quantitatively compare the photodissociation and crosslinking behavior of the different systems, reaction yields were estimated from the relative intensities of the fragment ions in the corresponding mass spectra. The photodissociation yield in UVPD-MS^2 was defined as the combined intensity of fragment ions associated with tetrazole photolysis relative to the total fragment ion intensity. The crosslinking yield in UVPD-CID-MS^3 was calculated as the combined intensity of diagnostic fragment ions originating from

macrocyclic crosslinked structures, including characteristic internal residue losses, relative to the total fragment ion intensity (Table 1).

In summary, the CID-MS^3 results indicate that the $[M+H-N_2]^+$ ions generated by UVPD are not simply denitrogenated products but undergo further intramolecular reactions to form crosslinked ions with common structural features, with most systems exhibiting appreciable yields. The highly similar fragmentation patterns across the different systems, together with the recurring phenylhydrazine and internal Ala residue losses, support the formation of macrocyclic nitrile-imine crosslinked structures. These structures were further evaluated using ion mobility mass spectrometry and theoretical calculations.

Yields		
Sequence	UVPD-MS^2	UVPD-CID-MS^3
FAAA-tet-K	53(99)	74
YAAA-tet-K	58	86
3-NO_2-YAAA-tet-K	25	92
YAAA-4-NO_2-tet-K	57	99
WAAA-tet-K	21(75)	93
5-OH-WAAA-tet-K	18	94
WAAA-4-OCH_3-tet-K	13	＜5

Table 1. Photodissociation and Crosslinking Yields

3.3 Ion Mobility Analysis and Conformational Effects

To further investigate whether stable intramolecular aromatic interactions exist between the aromatic side chains and diaryltetrazole groups, cyclic traveling-wave ion mobility mass spectrometry (cIMS-MS) was combined with theoretical calculations to analyze the gas-phase conformations of the precursor ions and their denitrogenated products.

The calculated collision cross sections (CCS_{calc}) of the low-energy structures were generally in good agreement with the experimentally measured values (CCS_{exp}), indicating that the calculated conformations reasonably represented the gas-phase ion structures. Although the CCS values varied among the systems, the ions generally adopted relatively compact, folded conformations, suggesting that these tetrazole–peptide ions can form intramolecular interactions and maintain specific spatial arrangements in the gas phase. The experimental CCS values, theoretical results, and corresponding structural features of the major systems are summarized in Table 2.

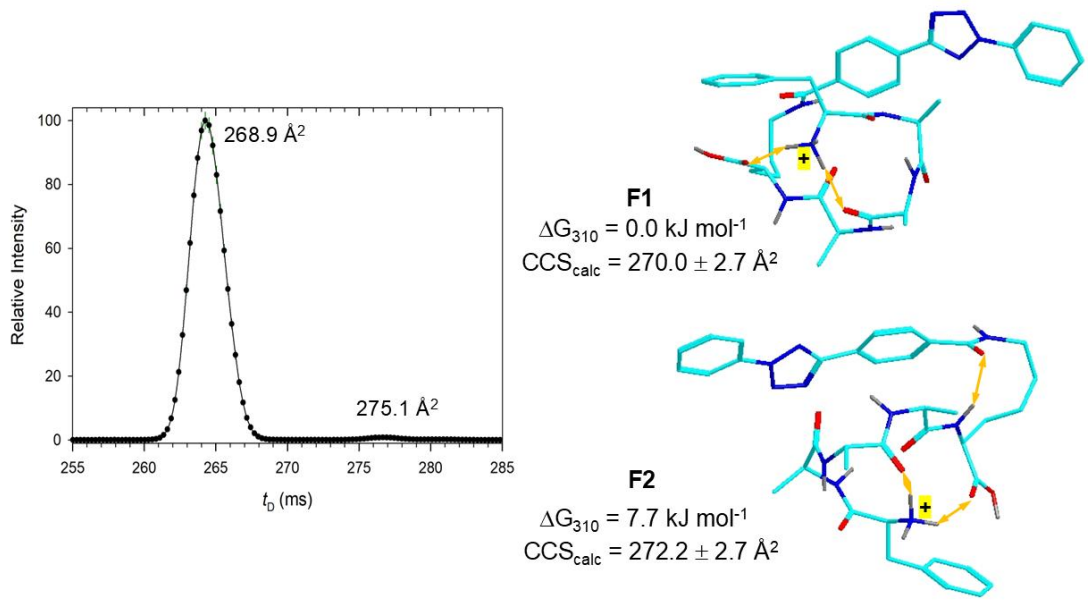

Figure 10. Ion mobility profile and low-energy conformers of FAAA-tet-K.

Peptide ion	CCSexp (Å²)	Lowest-Energy CCScalc (Å²)	Structural features	π – π stacking
FAAA-tet-K	268.9	270.0 / 272.2	Compact, H-bonded	Not observed
YAAA-tet-K	271.6	272.2	Folded	Not observed
WAAA-tet-K	277.0	276.6	Compact	No persistent stacking
3-NO_2-YAAA-tet-K	270.0 (99%); 279.0 (1%)	280.7	Experiment–calculation mismatch	Possible in calculations

Table 2. Calculated and experimental CCS values and structural features of tetrazole–peptide conjugates.

Notably, for 3-NO_2-YAAA-tet-K, the CCS of the major experimental peak deviated substantially from that calculated for the lowest-energy conformer. This discrepancy indicates that the predominant gas-phase conformation observed experimentally may not correspond to the thermodynamically lowest-energy structure and suggests the possible presence of multiple conformations or conformational dynamics. Therefore, structural assignment of this system cannot be based solely on the lowest-energy DFT conformer but requires an integrated analysis of both experimental and computational results.

In addition, the $(M-N_2+H)^+$ ions were analyzed by high-resolution ion mobility mass spectrometry (Figure 11). The CCS_{exp} values of the major peaks for the denitrogenated products of FAAA-tet-K, YAAA-tet-K, and WAAA-tet-K were lower than those of their corresponding precursor ions, indicating structural compression of approximately 1.7–2.7% following N_2 loss. In contrast, the calculated noncyclized, extended nitrile-imine conformations had substantially larger CCS_{calc} values and therefore could not account for the major experimental mobility components. Together with the sequential internal residue losses

observed by CID-MS³, these results further support the assignment of the major denitrogenated products as compact macrocyclic crosslinked structures. The 3-NO_2-YAAA-tet-K system was an exception, as the CCS_{exp} of its denitrogenated product was slightly larger than that of its precursor, suggesting that different systems may undergo distinct conformational rearrangements following cyclization.

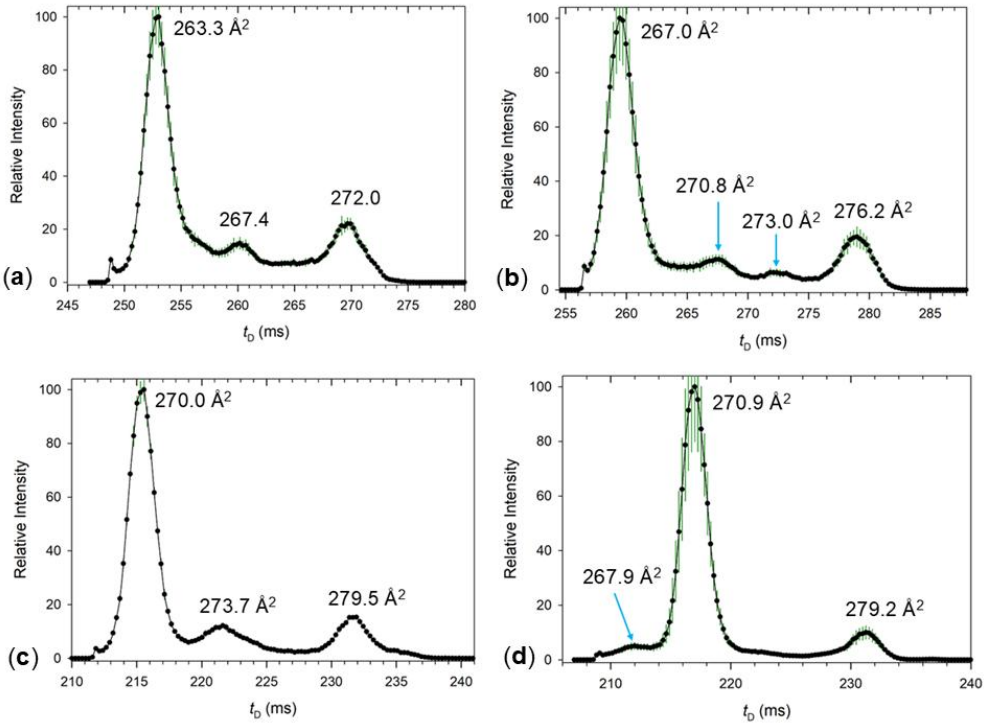

Figure 11. Ion mobility profiles of denitrogenated tetrazole–peptide conjugates: (a) FAAA-tet-K, (b) YAAA-tet-K, (c) WAAA-tet-K, and (d) 3-NO_2-YAAA-tet-K

However, further analysis of these low-energy structures showed that the major experimentally relevant conformers did not exhibit stable aromatic ring stacking. Although the aromatic side chains and tetrazole rings were in relatively close proximity in some structures, their distances and orientations generally did not meet the criteria for typical π–π stacking interactions. Therefore, the optimized structures provided no evidence that stable ground-state aromatic stacking is a general feature of these systems.

To further examine the dynamic conformational behavior of these systems, Born–Oppenheimer molecular dynamics (BOMD) simulations were performed for representative systems. The BOMD results showed that the distances between the aromatic side chains and diaryltetrazole rings varied continuously throughout the simulations. For WAAA-tet-K, frequent dynamic contacts occurred between the Trp side chain and diaryltetrazole moiety; however, these contacts did not form a single, stable π–π-stacked ground-state conformer that persisted over time.

Further comparison of systems containing different aromatic residues showed that Trp, owing to its larger π-conjugated system, would theoretically be more likely to form aromatic interactions with diaryltetrazole. However, even for WAAA-tet-K, no stable aromatic ring-stacked conformer that persisted over time was observed. Although the NO_2-substituted systems exhibited different electronic properties and some calculated low-energy structures of 3-NO_2-YAAA-tet-K showed aromatic ring stacking, the CCS_calc of the lowest-energy conformer did not match the major experimental peak. Therefore, stable π–π stacking cannot be considered a general or predominant conformational feature of these conjugates.

Taken together, the ion mobility measurements, low-energy structural analyses, and BOMD simulations indicate that stable ground-state aromatic stacking is not a predominant conformational feature of the systems investigated in this study. Although transient spatial proximity may occur between the aromatic side chains and diaryltetrazole groups, no clear correlation was observed between ground-state π–π stacking and either UVPD behavior or crosslinking yields across the different systems. Therefore, the effects of aromatic residues on

tetrazole photochemistry are more likely attributable to other factors, such as excited-state electronic structures and energy-distribution processes following photoexcitation.

3.4 Computational Analysis of Excited-State Electronic Structures

To further understand the origins of the differences in UVPD behavior among the aromatic systems, density functional theory (DFT) and time-dependent density functional theory (TD-DFT) were used to analyze their low-energy structures and excited-state electronic properties.

The DFT results revealed multiple low-energy conformers with similar energies for each system, indicating a degree of conformational flexibility among the charged peptide ions in the gas phase. When considered together with the ion mobility results described above, the major experimentally observed conformations were reasonably accounted for by the corresponding low-energy structures (Figure 10). However, these ground-state conformational features showed no direct correlation with the observed UVPD fragmentation behavior. Therefore, differences in ground-state conformations are unlikely to be the primary factor governing the variations in UVPD behavior among the systems.

In contrast, the TD-DFT results showed that different aromatic residues and substituents affected the excited-state electronic structures of the tetrazole–peptide conjugates. As shown in Figure 12, the major electronic transitions in the 250–280 nm range were generally associated with the diaryltetrazole chromophore, whereas aromatic side chains such as Tyr and Trp could also contribute to the electronic distribution in higher-energy excited states. These results are consistent with the experimentally observed wavelength-dependent UVPD

behavior: excitation at longer wavelengths predominantly promoted tetrazole N_2 loss, whereas excitation at 213 nm more readily induced competing peptide backbone fragmentation.

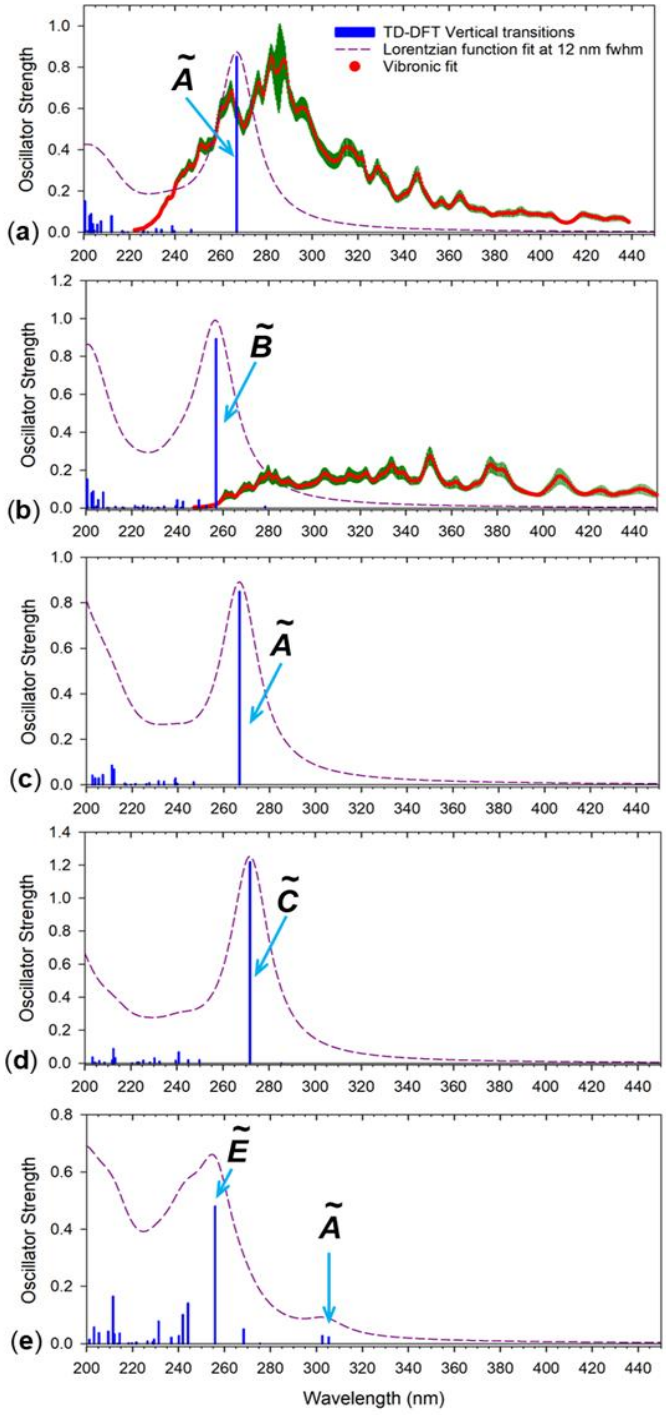

Figure 12. TD-DFT absorption spectra of tetrazole–peptide conjugates: (a) FAAA-tet-K, (b) WAAA-tet-K, (c) YAAA-tet-K, (d) YAAA-4-NO_2-tet-K, and (e) 3-NO_2-YAAA-tet-K.

In the WAAA-tet-K system, however, the Trp side chain contributed more substantially to the electronic structures of certain excited states. The TD-DFT results showed that some electronic transitions involved charge transfer from the Trp π orbitals to the diaryltetrazole π* orbitals, indicating that the Trp side chain participated in the electronic redistribution following photoexcitation. This excited-state behavior may be related to the experimentally observed competition among N_2 loss, backbone cleavage, and Trp side-chain fragmentation (Figure 13 and Table 3).

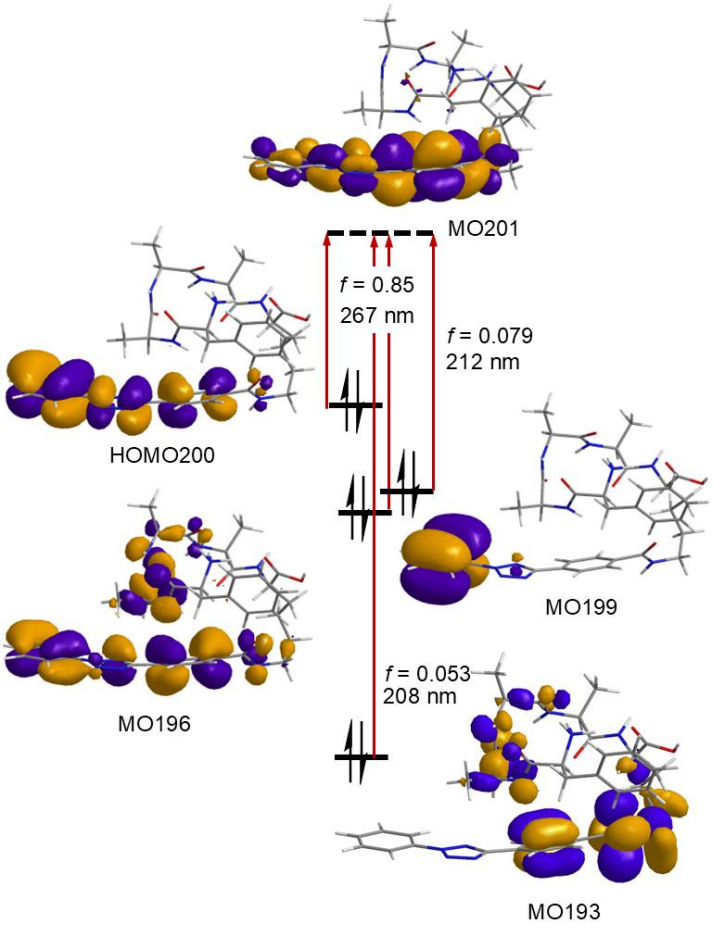

Figure 13. Electronic transitions and molecular orbitals of FAAA-tet-K.

Peptide ion	Major excitation character	Aromatic residue involvement	Possible relevance to UVPD
FAAA-tet-K	Mainly diaryltetrazole π→π* excitation	Weak	Consistent with selective N_2 loss at 250–280 nm
YAAA-tet-K	Diaryltetrazole and Tyr-related transitions	Moderate	Tyr contributes to some higher-energy excited states
WAAA-tet-K	Trp π system participates in electronic transitions	Strong	May contribute to competing fragmentation pathways
YAAA-4-NO_2-tet-K	Diaryltetrazole π→π* at 250–280 nm; mixed Tyr/charge-transfer states near 213 nm	Significant	Substituent modifies the excited-state distribution
3-NO_2-YAAA-tet-K	Mixed transitions involving nitrotyrosine and diaryltetrazole orbitals	Significant	Indicates stronger electronic coupling between the aromatic systems

Table 3. Excited-state characteristics of tetrazole–peptide conjugates.

The TD-DFT results for the NO_2-substituted systems further showed that substituents can alter the electronic distributions and associated excited-state properties of diaryltetrazole conjugates. For YAAA-4-NO_2-tet-K, the major absorptions in the 250–280 nm range were still dominated by π–π* transitions within the nitro-substituted diaryltetrazole system, whereas the excited states near 213 nm exhibited mixed characteristics involving transitions within the Tyr aromatic ring and charge transfer. The 3-NO_2-YAAA-tet-K system also displayed relatively complex orbital coupling between its aromatic systems. Although these differences may affect the specific photoexcitation processes, they showed no simple direct correlation with crosslinking yields.

Taken together, the TD-DFT results and wavelength-dependent UVPD experiments indicate that the initial photodissociation and competing fragmentation behavior at different excitation wavelengths are closely related to the types of electronic transitions involved.

Excitation at 250–280 nm primarily targets the diaryltetrazole chromophore and selectively promotes N_2 loss, whereas excitation at 213 nm accesses higher-energy and more complex electronic states and therefore more readily induces concurrent peptide backbone fragmentation. However, these excited-state differences mainly account for the initial photodissociation behavior, and the current results do not indicate that any particular type of electronic transition universally determines the crosslinking yield following N_2 loss.

3.5 Mechanistic Implications for Gas-Phase Nitrile-Imine Crosslinking

Taken together, the UVPD-MS^2, CID-MS^3, ion mobility mass spectrometry, and theoretical results described above provide further insight into the effects of aromatic amino acid residues on the gas-phase photochemical behavior of tetrazole–peptide conjugates and their nitrile-imine crosslinking processes.

The UVPD experiments showed that the tetrazole group efficiently underwent N_2 loss upon UV excitation, generating highly reactive nitrile-imine intermediates that subsequently participated in intramolecular reactions. Characteristic fragmentation behavior observed in the CID-MS^3 analysis, including sequential amino acid residue losses, further supported the formation of macrocyclic crosslinked structures (Figure 14), indicating that the nitrile imines generated by tetrazole photolysis can react efficiently with peptide backbone amide groups in the gas phase. The similar crosslinking characteristics observed across the different aromatic systems suggest that this reaction is primarily driven by the intrinsic high reactivity of the nitrile-imine intermediate rather than being determined solely by the structure of a specific aromatic residue.

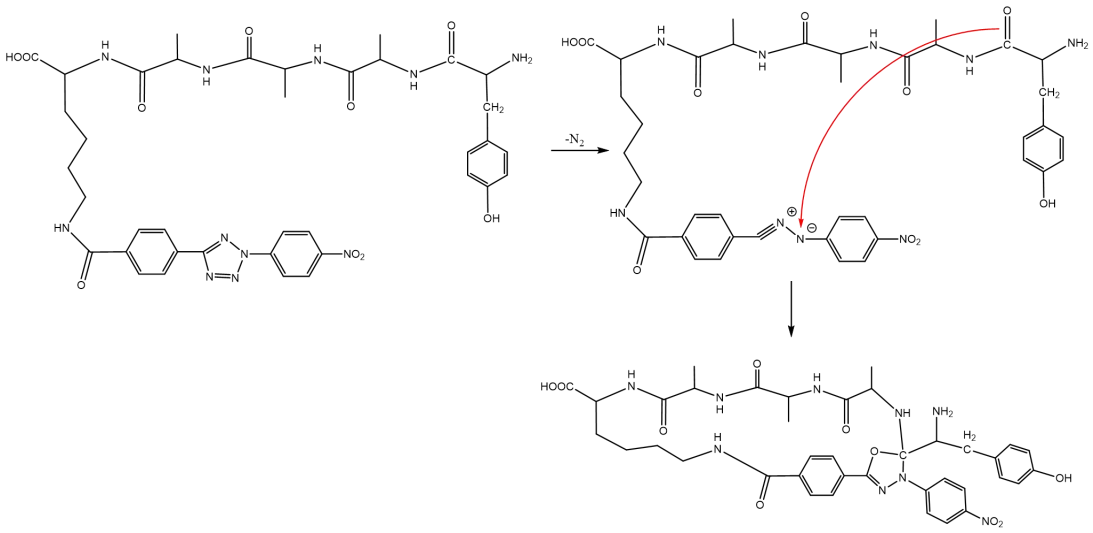

Figure 14. Proposed pathway for nitrile-imine-mediated macrocyclization.

This study initially hypothesized that π–π stacking between the aromatic side chains and tetrazole rings could influence the photochemical processes. However, the ion mobility measurements, low-energy structural analyses, and BOMD simulations showed that stable ground-state aromatic stacking was not a predominant conformational feature in most systems. Although relatively close contacts or local stacking tendencies between the aromatic rings may occur in some systems, particularly those containing nitro substituents, such interactions were not consistently observed across all systems and could not be directly correlated with differences in their UVPD behavior. Therefore, stable π–π stacking cannot serve as the primary explanation for the variations in UVPD behavior observed in this study.

WAAA-4-OCH_3-tet-K exhibited reaction behavior markedly different from that of the other tetrazole–peptide conjugates. This system produced a greater abundance of peptide backbone fragments upon UVPD and underwent subsequent neutral loss of 4-methoxyaniline following N_2 loss, generating a product ion at m/z 673. CID-MS^3 predominantly produced conventional b-type fragment ions, indicating that the m/z 673 ion retained a linear peptide

backbone rather than adopting a typical macrocyclic crosslinked structure. Its crosslinking yield in UVPD-CID-MS³ was below 5%, making it the most notable exception in this study. According to the proposed mechanism, the electron-donating effect of the OMe substituent may stabilize the iminium intermediate formed following N–N bond cleavage, thereby promoting 4-methoxyaniline loss. Although this interpretation remains a tentative mechanistic assignment, it suggests that substituent electronic effects can substantially alter the subsequent reaction pathways of nitrile-imine intermediates in specific systems.

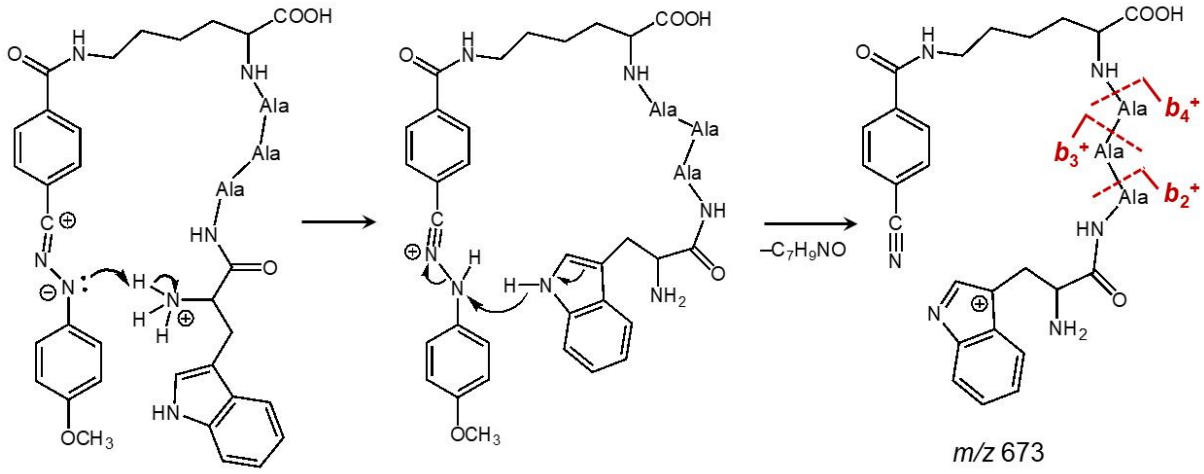

Figure 15. Formation and backbone cleavage of the m/z 673 ion.

The TD-DFT results further showed that different aromatic residues can participate in or modulate the excited-state electronic distributions of tetrazole–peptide conjugates. Excitation at 250–280 nm primarily corresponds to π–π* transitions within the diaryltetrazole chromophore and therefore enhances the selectivity of tetrazole N_2 loss. In contrast, the higher-energy excited states near 213 nm may involve both the aromatic amino acid side chains and the diaryltetrazole system, resulting in competition between N_2 loss and peptide backbone cleavage. These results explain the differences in primary photodissociation

behavior at different wavelengths; however, no simple correlation was observed between these excited-state characteristics and the crosslinking yields following N_2 loss.

Therefore, the present study supports the following reaction model: upon UV excitation, tetrazole–peptide conjugates undergo N_2 loss to generate highly reactive nitrile-imine intermediates. Most of these intermediates subsequently undergo intramolecular reactions with peptide backbone amides to form macrocyclic crosslinked ions. Stable ground-state π–π stacking is not required for this cyclization process, whereas the electronic properties of different aromatic residues and substituents primarily affect photoexcitation and competing fragmentation pathways. In specific systems such as WAAA-4-OCH_3-tet-K, substituent electronic effects may also alter the subsequent reactions of the nitrile-imine intermediate, allowing competing fragmentation to predominate over macrocycle formation. Overall, these results demonstrate that ground-state conformation, excited-state photodissociation, and post-N_2-loss crosslinking are interconnected but distinct processes.

Chapter 4. Conclusion

In this study, a series of diaryltetrazole-modified peptides containing aromatic amino acid residues were used as model systems. Ultraviolet photodissociation mass spectrometry (UVPD-MS), collision-induced dissociation mass spectrometry (CID-MS^3), high-resolution ion mobility mass spectrometry (IM-MS), and theoretical calculations were combined to systematically investigate the structural basis and photochemical behavior of gas-phase nitrile-imine crosslinking reactions.

The experimental results showed that tetrazole N_2 loss occurred in all systems upon UV irradiation, generating highly reactive nitrile-imine intermediates, although their relative abundances were influenced by the excitation wavelength and molecular structure. Most N_2-loss intermediates subsequently underwent intramolecular reactions with peptide backbone amides to form macrocyclic crosslinked ions. The major crosslinked products and their characteristic fragmentation behavior were successfully characterized using UVPD-MS^2, CID-MS^3, and high-resolution accurate mass measurements, and the corresponding fragmentation mechanisms and structural models were further proposed.

The ion mobility experiments and theoretical calculations showed that, although transient contacts or weak interactions may occur between the aromatic amino acid side chains and diaryltetrazole rings, stable and persistent ground-state π–π-stacked structures were not observed in most systems. The experimentally measured collision cross sections were in good agreement with the theoretical results, further supporting the proposed gas-phase

conformational models. Therefore, these findings indicate that stable ground-state aromatic stacking is not required for gas-phase nitrile-imine crosslinking.

Wavelength-dependent UVPD experiments and TD-DFT analyses showed that the excitation wavelength and corresponding types of electronic transitions influenced the competition between tetrazole N_2 loss and peptide backbone cleavage. In the 250–280 nm range, the dominant excitations involved π–π* transitions within the diaryltetrazole chromophore, thereby increasing the selectivity of tetrazole photodissociation. In contrast, excitation at 213 nm involved higher-energy and more complex electronic states in which the aromatic amino acid side chains could participate. Importantly, these excited-state differences primarily account for the initial photodissociation behavior and did not show a general determining effect on subsequent crosslinking yields.

Overall, this study demonstrates that stable ground-state π–π stacking is not required for efficient nitrile-imine crosslinking. Most tetrazole–peptide conjugates formed macrocyclic crosslinked ions in high proportions following N_2 loss, whereas WAAA-4-OCH_3-tet-K exhibited substantial competing fragmentation, suggesting that substituent electronic effects may alter the subsequent reaction pathways of the intermediate in specific systems. By distinguishing among ground-state conformation, photoexcitation, and post-N_2-loss crosslinking, this study further refines the mechanistic understanding of gas-phase nitrile-imine reactions.

Future studies could extend this approach to nucleic acid, protein, and intermolecular crosslinking systems. More detailed excited-state dynamics calculations and

wavelength-selective investigations could further enable precise control over the selectivity and reaction pathways of photochemical crosslinking.

Chapter 5. Acknowledgements

I would like to acknowledge the Chemistry Division of the U.S. National Science Foundation for supporting this research at the University of Washington. I am also grateful for the additional support provided by the Klaus and Mary Ann Saegebarth Endowment.

Bibliography

1. Ollis, D. L.; White, S. W. Structural basis of protein-nucleic acid interactions. Chemical Reviews 1987, 87 (5), 981–995. https://doi.org/10.1021/cr00081a006
2. Piersimoni, L.; Kastritis, P. L.; Arlt, C.; Sinz, A. Cross-linking mass spectrometry for investigating protein conformations and protein–protein interactions—A method for all seasons. Chemical Reviews 2022, 122, 7500–7531. https://doi.org/10.1021/acs.chemrev.1c00786
3. Wong, S. S.; Wong, L. C. Chemical crosslinking and the stabilization of proteins and enzymes. Enzyme and Microbial Technology 1992, 14 (11), 866–874. https://doi.org/10.1016/0141-0229(92)90049-T
4. Preston, G. W.; Wilson, A. J. Photo-induced covalent cross-linking for the analysis of biomolecular interactions. Chemical Society Reviews 2013, 42, 3289–3301. https://doi.org/10.1039/C3CS35459H
5. Hennink, W. E.; van Nostrum, C. F. Novel crosslinking methods to design hydrogels. Advanced Drug Delivery Reviews 2012, 64, 223–236. https://doi.org/10.1016/j.addr.2012.09.009
6. Jayachandran, B.; Parvin, T. N.; Alam, M. M.; Chanda, K.; MM, B. Insights on chemical crosslinking strategies for proteins. Molecules 2022, 27 (23), 8124. https://doi.org/10.3390/molecules27238124
7. Lim, K. S.; Galarraga, J. H.; Cui, X.; Lindberg, G. C. J.; Burdick, J. A.; Woodfield, T. B. F. Fundamentals and applications of photo-cross-linking in bioprinting. Chemical Reviews 2020, 120 (19), 10662–10694. https://doi.org/10.1021/acs.chemrev.9b00812

8. Tureček, F. Covalent crosslinking in gas-phase biomolecular ions: An account and perspective. Physical Chemistry Chemical Physics 2023, 25, 32292–32304. https://doi.org/10.1039/D3CP04879A
9. Bitan, G.; Teplow, D. B. Rapid photochemical cross-linking—A new tool for studies of metastable, amyloidogenic protein assemblies. Accounts of Chemical Research 2004, 37 (6), 357–364. https://doi.org/10.1021/ar000214l
10. Das, J. Aliphatic diazirines as photoaffinity probes for proteins: Recent developments. Chemical Reviews 2011, 111 (8), 4405–4417. https://doi.org/10.1021/cr1002722
11. Roth, A. D.; Thamattoor, D. M. Carbenes from cyclopropanated aromatics. Organic & Biomolecular Chemistry 2023, 21, 9482–9506. https://doi.org/10.1039/d3ob01525d
12. Shawali, A. S. Reactions of heterocyclic compounds with nitrilimines and their precursors. Chemical Reviews 1993, 93, 2731–2777. https://doi.org/10.1021/cr00024a007
13. Song, W.; Wang, Y.; Qu, J.; Madden, M. M.; Lin, Q. A photoinducible 1,3-dipolar cycloaddition reaction for rapid, selective modification of tetrazole-containing proteins. Angewandte Chemie 2008, 120 (15), 2874–2877. https://doi.org/10.1002/ange.200705805
14. Zhang, J.; Liu, J.; Li, X.; Ju, Y.; Li, Y.; Zhang, G.; Li, Y. Unexpected cyclization product discovery from the photoinduced bioconjugation chemistry between tetrazole and amine. Journal of the American Chemical Society 2024, 146, 2122–2131. https://doi.org/10.1021/jacs.3c11574
15. Zhao, S.; Dai, J.; Hu, M.; Liu, C.; Meng, R.; Liu, X.; Wang, C.; Luo, T. Photo-induced coupling reactions of tetrazoles with carboxylic acids in aqueous solution: Application in

protein labelling. Chemical Communications 2016, 52, 4702–4705. https://doi.org/10.1039/C5CC10445A

16. Herner, A.; Marjanovic, J.; Lewandowski, T. M.; Marin, V.; Patterson, M.; Miesbauer, L.; Ready, D.; Williams, J.; Vasudevan, A.; Lin, Q. 2-Aryl-5-carboxytetrazole as a new photoaffinity label for drug target identification. Journal of the American Chemical Society 2016, 138, 14609–14615. https://doi.org/10.1021/jacs.6b06645
17. Tian, Y.; Jacinto, M. P.; Zeng, Y.; Yu, Z.; Qu, J.; Liu, W. R.; Lin, Q. Genetically encoded 2-aryl-5-carboxytetrazoles for site-selective protein photo-cross-linking. Journal of the American Chemical Society 2017, 139, 6078–6081. https://doi.org/10.1021/jacs.7b01321
18. Neagu, A.-N.; Jayathirtha, M.; Baxter, E.; Donnelly, M.; Petre, B. A.; Darie, C. C. Applications of tandem mass spectrometry (MS/MS) in protein analysis for biomedical research. Molecules 2022, 27 (8), 2411. https://doi.org/10.3390/molecules27082411
19. Larsen, M. R.; Trelle, M. B.; Thingholm, T. E.; Jensen, O. N. Analysis of posttranslational modifications of proteins by tandem mass spectrometry. BioTechniques 2006, 40 (6), 790–798. https://doi.org/10.2144/000112201
20. Yu, C.; Huang, L. Cross-linking mass spectrometry (XL-MS): An emerging technology for interactomics and structural biology. Analytical Chemistry 2018, 90 (1), 144–165. https://doi.org/10.1021/acs.analchem.7b04431
21. Singh, P.; Panchaud, A.; Goodlett, D. R. Chemical cross-linking and mass spectrometry as a low-resolution protein structure determination technique. Analytical Chemistry 2010, 82 (7), 2636–2642. https://doi.org/10.1021/ac1000724

22. Wan, J.; Nytka, M.; Qian, H.; Vu, K.; Lemr, K.; Tureček, F. Nitrile imines as peptide and oligonucleotide photo-cross-linkers in gas-phase ions. Journal of the American Society for Mass Spectrometry 2024, 35, 344–356. https://doi.org/10.1021/jasms.3c00379

23. Vlk, M.; Wan, J.; Nytka, M.; Vu, T. N. K.; Lemr, K.; Tureček, F. Photochemical and collision-induced cross-linking of Asp, Glu, Asn, and Gln residues in peptide-nitrile imine conjugate ions in the gas phase. Journal of the American Society for Mass Spectrometry 2025, 36, 175–186. https://doi.org/10.1021/jasms.4c00394

24. Dai, C.; Shen, S.; Halman, D.; Sedláčková, S.; Lemr, K.; Tureček, F. Nitrile-imine cross-linking in peptide ions with aromatic amino acid residues: Are ring-stacking interactions important? Journal of the American Society for Mass Spectrometry 2026, 37 (2), 556–569. https://doi.org/10.1021/jasms.5c00449

25. Calinsky, R.; Levy, Y. Aromatic residues in proteins: Re-evaluating the geometry and energetics of π–π, cation–π, and CH–π interactions. The Journal of Physical Chemistry B 2024, 128, 8687–8700. https://doi.org/10.1021/acs.jpcb.4c04774

26. Creaser, C. S.; Griffiths, J. R.; Bramwell, C. J.; Noreen, S.; Hill, C. A.; Thomas, C. L. P. Ion mobility spectrometry: A review. Part 1. Structural analysis by mobility measurement. Analyst 2004, 129, 984–994. https://doi.org/10.1039/B404531A

27. Bohrer, B. C.; Merenbloom, S. I.; Koeniger, S. L.; Hilderbrand, A. E.; Clemmer, D. E. Biomolecule analysis by ion mobility spectrometry. Annual Review of Analytical Chemistry 2008, 1, 293–327.

28. Girod, M.; Sanader, Z.; Vojkovic, M.; Antoine, R.; MacAleese, L.; Lemoine, J.; Bonacic-Koutecky, V.; Dugourd, P. UV photodissociation of proline-containing peptide ions:

Insights from molecular dynamics. Journal of the American Society for Mass Spectrometry 2015, 26 (3), 432–443. https://doi.org/10.1007/s13361-014-1038-1

29. Wang, S.-S. p-Alkoxybenzyl alcohol resin and p-alkoxybenzyloxycarbonylhydrazide resin for solid-phase synthesis of protected peptide fragments. Journal of the American Chemical Society 1973, 95 (4), 1328–1333. https://doi.org/10.1021/ja00785a602